AGU PUBLICATIONS

Water Resources Research

RESEARCH ARTICLE
10.1002/2017WR020793

The potential of GRACE gravimetry to detect the heavy rainfall-induced impoundment of a small reservoir in the upper Yellow River

Shuang Yi[1,2], Chunqiao Song[3], Qiuyu Wang[2], Linsong Wang[4], Kosuke Heki[1], and Wenke Sun[2]

[1]Department of Earth and Planetary Sciences, Hokkaido University, Sapporo, Japan, [2]Key Laboratory of Computational Geodynamics, University of Chinese Academy of Sciences, Beijing, China, [3]Department of Geography, University of California, Los Angeles, Los Angeles, California, USA, [4]Institute of Geophysics and Geomatics, China University of Geosciences, Wuhan, China

Key Points:
- Intense precipitation in 2005 caused the Longyangxia Reservoir to experience increases of 37.9 m in water level and 13 Gt in mass
- Mass changes in this ~400 km^2 reservoir can be detected by GRACE gravity satellite data
- A signal of small size can potentially be detected by the GRACE, given that its mass change is larger than 6 Gt

Supporting Information:
- Supporting Information S1

Correspondence to:
S. Yi,
shuangyi.geo@gmail.com

Citation:
Yi, S., C. Song, Q. Wang, L. Wang, K. Heki, and W. Sun (2017), The potential of GRACE gravimetry to detect the heavy rainfall-induced impoundment of a small reservoir in the upper Yellow River, *Water Resour. Res.*, *53*, doi:10.1002/2017WR020793.

Received 20 MAR 2017
Accepted 7 JUL 2017
Accepted article online 13 JUL 2017

Abstract Artificial reservoirs are important indicators of anthropogenic impacts on environments, and their cumulative influences on the local water storage will change the gravity signal. However, because of their small signal size, such gravity changes are seldom studied using satellite gravimetry from the Gravity Recovery and Climate Experiment (GRACE). Here we investigate the ability of GRACE to detect water storage changes in the Longyangxia Reservoir (LR), which is situated in the upper main stem of the Yellow River. Three different GRACE solutions from the CSR, GFZ, and JPL with three different processing filters are compared here. We find that heavy precipitation in the summer of 2005 caused the LR water storage to increase by 37.9 m in height, which is equivalent to 13.0 Gt in mass, and that the CSR solutions with a DDK4 filter show the best performance in revealing the synthetic gravity signals. We also obtain 109 pairs of reservoir inundation area measurements from satellite imagery and water level changes from laser altimetry and in situ observations to derive the area-height ratios for the LR. The root mean square of GRACE series in the LR is reduced by 39% after removing synthetic signals caused by mass changes in the LR or by 62% if the GRACE series is further smoothed. We conclude that GRACE data show promising potential in detecting water storage changes in this ~400 km^2 reservoir and that a small signal size is not a restricting factor for detection using GRACE data.

Plain Language Summary Changes in water resource, which are strongly correlated with the sustaining development of society and economy, are attracting wide public concerns. Building of dams and reservoirs is a main way for humans to control the water resource. The changes in water volume (i.e., changes in mass) will cause a gravity increase or decrease, which could be detected by gravity satellites in the space on the condition that the gravity signal is large enough. Up to now, space gravity is only used to study water volume changes in the Three Gorges Reservoir, which is the largest hydroelectric power station in the world. Here we demonstrate that the potential of applying space gravity measurements to detect the hydrologic regime of another reservoir in a much smaller size, the Longyangxia Reservoir, located in the upper stream of the Yellow River, China.

1. Introduction

Gravity Recovery and Climate Experiment (GRACE) observations have been widely adopted to study the impact of climate change and of anthropogenic activities on the water system, including polar ice sheets [*Velicogna and Wahr*, 2006; *Chen et al.*, 2009; *Gardner et al.*, 2013], mountain glaciers [*Matsuo and Heki*, 2010; *Yi and Sun*, 2014; *Farinotti et al.*, 2015; *Song et al.*, 2015; *Yi et al.*, 2016b], terrestrial water storage (e.g., groundwater [*Rodell et al.*, 2009; *Famiglietti et al.*, 2011; *Voss et al.*, 2013; *Chen et al.*, 2016; *Xiang et al.*, 2016], large inland water bodies [*Swenson and Wahr*, 2009; *Becker et al.*, 2010; *Singh et al.*, 2012], and soil water content [*Landerer and Swenson*, 2012; *Long et al.*, 2015; *Yi et al.*, 2016c]) and global sea level changes [*Cazenave et al.*, 2009; *Boening et al.*, 2012; *Chen et al.*, 2013; *Yi et al.*, 2015]. In the application of GRACE products, a lot of attention has been paid to ice melting and groundwater depletion, as these signals are strong, cover

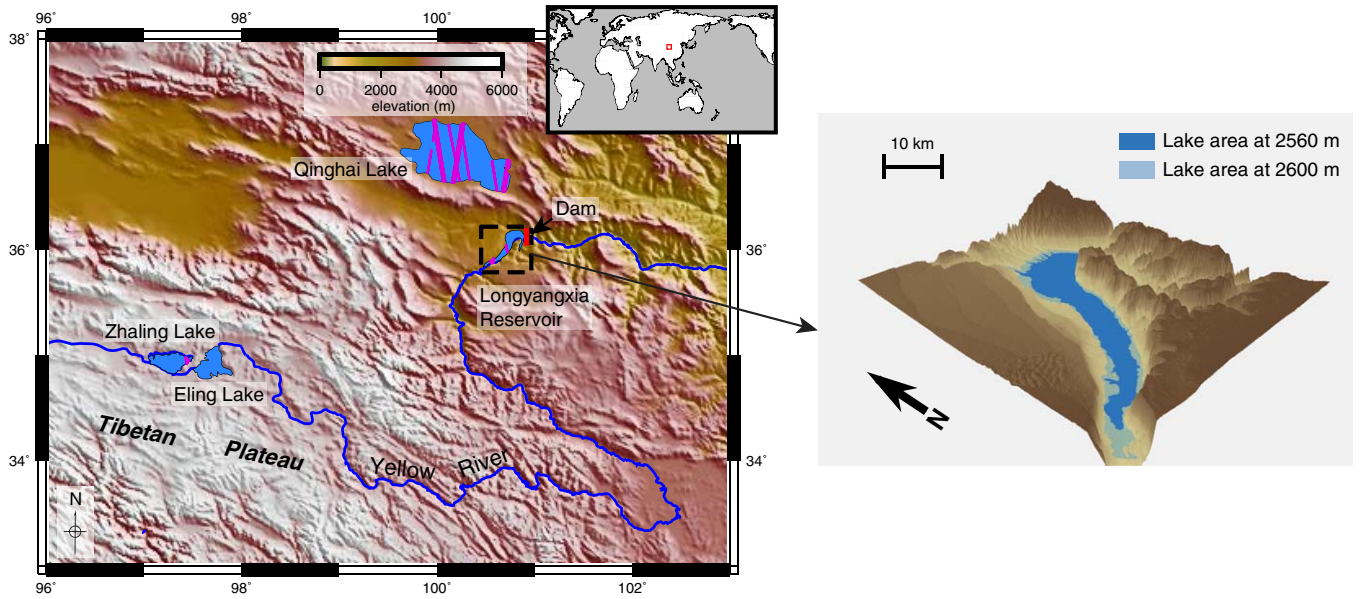

Figure 1. Geographical environment of the Longyangxia Reservoir (left) and its three-dimensional aerial view (right). The red bar indicates the location of the Longyangxia Dam, and the black dashed box shows the spatial range of the aerial view. The violet dots atop Qinghai Lake, Zhaling Lake, and the Longyangxia Reservoir represent ICESat (Ice, Cloud, and land Elevation Satellite) footprints. The spatial extent of the left plot is shown in the top right inset.

a wide spatial range, and are more likely to be detected by GRACE. However, very few studies have been devoted to reservoirs, whose spatial extents are much smaller. In this study, we will test whether GRACE can detect water storage changes in an ~400 km^2 reservoir in the upper main stem of the Yellow River.

The impacts of human activities on land water are represented by two contrasting effects on sea level rise: the positive contribution of land water loss due to excessive groundwater extraction and the negative contribution of water gains impounded within man-made reservoirs [*Church et al.*, 2013]. Capturing mass change in artificial reservoirs can help us precisely quantitate artificial impacts on the water system, including not only visible pondage changes but also water storage changes in neighboring environments via seepage, which can be difficult to evaluate comprehensively using traditional methods [*Chao et al.*, 2008]. Knowing how much water is impounded can also benefit our understanding of the global water distribution and global sea level change [*Yi et al.*, 2015; *Reager et al.*, 2016].

As the largest hydroelectric power station in the world, with a capacity of 39.3 km^3, the Three Gorges Reservoir (TGR), located in the middle main stem of the Yangtze River, is the only reservoir that has been studied using GRACE observations to date [*Wang et al.*, 2007, 2011]. Here we will investigate the potential of applying GRACE measurements to detect the hydrologic regime of another reservoir with a much smaller size, namely, the Longyangxia Reservoir (LR). The Longyangxia Hydropower Project is located at the entrance of the Longyangxia Canyon and is 1648 km from the source of the Yellow River, where the upper main stem of the Yellow River exits the Tibetan Plateau and drops rapidly in altitude (Figure 1). Within the Longyangxia Canyon, granite walls rise steeply to 200 m high, and the mouth of the canyon narrows sharply to 30 m in width, making this canyon an ideal place for the construction of a dam to generate hydropower. Completed in 1989, the construction of the Longyangxia Dam resulted in a reservoir with an area of approximately 383 km^2 (Longyangxia Hydropower Project, 2010, http://www.chincold.org.cn/dams/rootfiles/2010/07/20/1279253974093926-1279253974095162.pdf).

The LR is the fourth largest reservoir in China and the largest reservoir within the Yellow River by volume, with a maximal capacity of 27.6 km^3 (http://www.chincold.org.cn/dams/DamInformation/damsinchina/webinfo/2010/07/1279253973938211.htm). The LR has a smaller capacity, and its area is approximately one third of the area of the TGR. Two favorable conditions may allow the high potential to quantify its gravity effect. First, the annual precipitation is approximately 400 mm around the LR region, which is much lower than that of the TGR region (more than 1000 mm); therefore, the terrestrial water storage varies more weakly around the LR. Second, there is a smaller population distribution and fewer intensive irrigation

activities in the LR region compared to the middle main stem of the Yangtze River [*Huang et al*., 2015]. In addition, the water level of the LR increased dramatically in the summer of 2005, after which a large mass accumulation occurred. All these factors will facilitate its detection by GRACE. In fact, GRACE has already showed its ability to identify signals at sizes smaller than its resolution, i.e., ice melting in the Patagonia Icefield, which covers an area of ~17,200 km^2 [*Chen et al*., 2007], one sixth of the spatial resolution of GRACE. In this study, the area of the LR is only 1/250 of the spatial resolution.

This work is organized in three parts. First, the equivalent water height (EWH) variations of these four water bodies that were caused by the water impoundment event in 2005 are synthesized based on their water level changes. We focus on how to derive volume changes from height observations in the LR. Second, synthetic EWH changes are compared with various GRACE observations. Finally, monthly GRACE observations are presented, and we quantitatively estimate the uncertainty of GRACE observations.

2. Data and Methods

2.1. Water Level Records

The upper main stem of the Yellow River runs through two large water bodies: Zhaling Lake and Eling Lake. Qinghai Lake is the largest water body in China, and it is less than 100 km away from the LR. Therefore, these three lakes are also studied here. The lake level records used here include four data sources: ICESat laser altimetry, radar altimetry, in situ observations, and records collected from news reports. The ICESat satellite system implements laser altimetry, so it has a smaller footprint compared with radar altimetry (70 m compared with several kilometers); however, its observations are only available from 2003 to 2009 [*Schutz et al*., 2005]. ICESat data are available at http://icesat.gsfc.nasa.gov/icesat/ and are widely used for the study of lake levels [*Zhang et al*., 2011; *Song et al*., 2013; *Wang et al*., 2013; *Zhang et al*., 2013]. The processing method used in this study can be found in *Wang et al*. [2016]. The tracks of ICESat cover the LR, Qinghai Lake, and Zhaling Lake (refer to the violet dots in Figure 1) but do not traverse Eling Lake, whose observations are obtained from radar altimetry available in the Hydroweb database [*Crétaux et al*., 2011].

The in situ water level observations of the LR are unavailable to the public for confidential reasons, but we select water level records for the LR between 2005 and 2012 from the figures in *Lu* [2013] and between 1986 and 2000 from the figures in *Cao* [2004]. However, there are no data available from 2001 or 2002. We also collect a dozen news reports about its water levels, especially during the swelling stage in 2005 (see supporting information). Multiple data sources are used to verify and supplement each other.

To investigate the relationship between precipitation and water level changes in the LR, precipitation records during 1985–2010 are also taken from Global Precipitation Climatology Centre (GPCC) [*Schneider et al*., 2011] (available at http://www.esrl.noaa.gov/psd/data/gridded/tables/precipitation.html).

2.2. GRACE Gravimetry

Since its launch in 2002, GRACE has been providing global gravity solutions every month, although some months lack measurements. Original GRACE observations are mainly processed by three organizations: the CSR, GFZ, and JPL. These organizations have different solution methods and have thus generated slightly different products [*Bettadpur*, 2012], which can be accessed at the ICGEM website (http://icgem.gfz-potsdam.de/ICGEM/) [*Barthelmes and Köhler*, 2016]. Here all three products are compared in their ability to capture the expected signals. The geocenter terms (degree one coefficients) are missing in the original datasets, but they are added back in this study [*Swenson et al*., 2008]. We also replace the C_{20} coefficients with solutions using satellite laser ranging [*Cheng et al*., 2011], which is generally accepted, to improve their accuracy. We adopt three different kinds of smoothing methods to test the robustness of the expected signals: DDK4 [*Kusche et al*., 2009], a Gaussian filter with a radius of 300 km (G300), and a decorrelation filter P4M6 [*Swenson and Wahr*, 2006]. Usually, the last filter is combined with a Gaussian filter [e.g., *Chen et al*., 2007]. Here the combination of P4M6 and a 150 km Gaussian filter is referred to as P4M6+G150.

One form of a GRACE product is the spherical harmonic coefficient (SHC), which can be adopted to study changes in the geoid and in gravity caused by mass transportation. Another widely used form is the EWH, which assumes that mass is only transported on the surface of the earth and straightforwardly reflects how much the water column changes. The calculation of the EWH from the SHC can be found in *Wahr et al*. [1998]

$$h(\theta,\phi,t)=\frac{a\rho_{ave}}{3\rho_w}\sum_{l=0}^{N}\sum_{m=0}^{l}\tilde{P}_{lm}(\cos\theta)\frac{2l+1}{1+k_l}\left(C_{lm}^{t}\cos(m\phi)+S_{lm}^{t}\sin(m\phi)\right),$$

where C_{lm}^{t} and S_{lm}^{t} are monthly (t) GRACE products and are functions of degree (l) and order (m); θ and ϕ are the colatitude and longitude of the observation point; the parameters a and ρ_{ave} are the radius and average density of the earth, respectively; ρ_w is the density of water; $\tilde{P}_{lm}$ are the normalized associated Legendre functions; and k_l is a set of loading Love numbers. Degrees ranging from 0 to higher values represent spatial resolutions ranging from global to regional, and the degree is truncated at N in the equation. We can also solve C_{lm} and S_{lm} if the EWH change h is known, and this process is known as expansion.

2.3. Theoretical EWH for Changing Water Storage Levels

The surface area of the LR expands/shrinks substantially with a dramatic water level rise/drop. Thus, water level change information alone is not enough to estimate water volume changes. First, the relationship between the inundation area and water height (named the area-height relationship) should be obtained. There are two widely used methods. The first method is to combine inundation areas retrieved using satellite imagery with lake surface heights obtained by altimetry radar, laser, and lidar or from in situ observations. This method has been used to study river basins, lakes, and reservoirs [e.g., *Leon et al*., 2006; *Peng et al*., 2006; *Birkinshaw et al*., 2010; *Frappart et al*., 2010, 2011; *Duan and Bastiaanssen*, 2013; *Song et al*., 2013; *Zhang et al*., 2013]. The other method is based on synthetic surface areas inferred from topographic maps (e.g., a 30 m resolution digital elevation model collected by NASA's Shuttle Radar Topography Mission (SRTM) [*Farr et al*., 2007]), which is less frequently used [e.g., *Matgen et al*., 2007; *Pan et al*., 2013; *Tseng et al*., 2016] due to the scarce accessibility of lake bathymetry data, especially for remote regions or developing countries. Both methods have merits and demerits. The former method, which is based on imagery and height data, has high precision, but it requires two different intensive observations to be carried out during the same period. The latter method, which is based on topography, can only provide relationships above the lake level at the time as when the topography measurements were taken; otherwise, it requires bathymetric maps, which can require costly and lengthy fieldwork data acquisition using shipborne sonar sensors [*Peng et al*., 2006; *Duan and Bastiaanssen*, 2013]. However, this method is very straightforward and does not require water level or area observations. These two methods are independent and based on different principles, so they can be mutually verified or supplemented [e.g., *Medina et al*., 2010].

Here we adopt the first method to reconstruct the empirical equation (geometric relationship) between inundation areas derived from satellite images and water level heights obtained from satellite altimetry and in situ observations [*Duan and Bastiaanssen*, 2013; *Song et al*., 2013]. We use multitemporal cloud-free optical images from Landsat 5/7 to derive the time series for area changes of the LR. Multitemporal Landsat images between 2003 and 2010, which are available at the USGS (U.S. Geological Survey) website http://glovis.usgs.gov, are used. Since the reservoir is located in the overlapping region of two adjacent Landsat scenes (Path132/Row035 and Path133/Row035), we can obtain nearly twice the amount of images for the LR compared with other general places, and it is thus able to provide denser temporal-resolution observations of reservoir evolution. A two-step NDWI (normalized difference water index) threshold segmentation model is used to extract the inundation areas [*Li and Sheng*, 2012; *Wang et al*., 2014]. The NDWI map is generated by the normalized water index between the green and near-infrared spectral bands; this process was developed by *McFeeters* [1996]. More details regarding water body mapping methodologies and procedures can be obtained from prior literature [*Sheng et al*., 2016; *Song and Sheng*, 2016]. For the other three lakes, the lake areas do not vary considerably, and thus, we simply add an extra 10% mass due to the surface expansion [*Wang et al*., 2016].

After we obtain these images and contemporary height records, we linearly interpolate the height records to obtain height information at the time when these 141 images were taken. However, we eliminate images taken at the time when no height observation is available within 15 days because the interpolated height information is likely to be unreliable under this condition. Finally, these combinations are used to derive the area-height relationship in the LR.

Once we determine the amount of rising water levels in these four water bodies and the accompanying area change, their theoretical EWHs caused by water storage changes can be estimated. First, we construct a set of grids with a resolution of 0.02° × 0.02° (which is known as a mask) to mark the location and shape

of each water body. Second, grids within the range of a water body are set to a uniform value to make their total mass equal to that of our observations, and those outside the range of a water body are set to zero. Because of the low spatial resolution of GRACE observations, these synthetic observations in terms of the EWH are expanded into SHCs, truncated to degree 60 (T60), and processed with the same procedures as are conducted on GRACE. The relevant equations were introduced in detail in *Wahr et al*. [1998].

3. Results and Analyses

3.1. Dramatic Reservoir Water Impoundment Detected by Satellite Altimetry and Imagery

3.1.1. Water Level Changes in the LR and Surrounding Lakes

Water level records of the four studied water bodies from the four types of data sources are shown in Figure 2 and in Table 1. These independent data sets agree well with each other. The in situ water level records of the LR are only available from 2005 on, and before that, only four records are available: three from ICESat and one from a news report. The most noticeable feature is the rapid rise in the water level from May to November in 2005. A total rise of 37.9 m occurred over half a year, with an average rising rate of over 0.2 m/d. Another less evident rise occurred in 2009. Apart from these two rising events, the water level presented either a balanced or a declining trend and was accompanied by large seasonal variations,

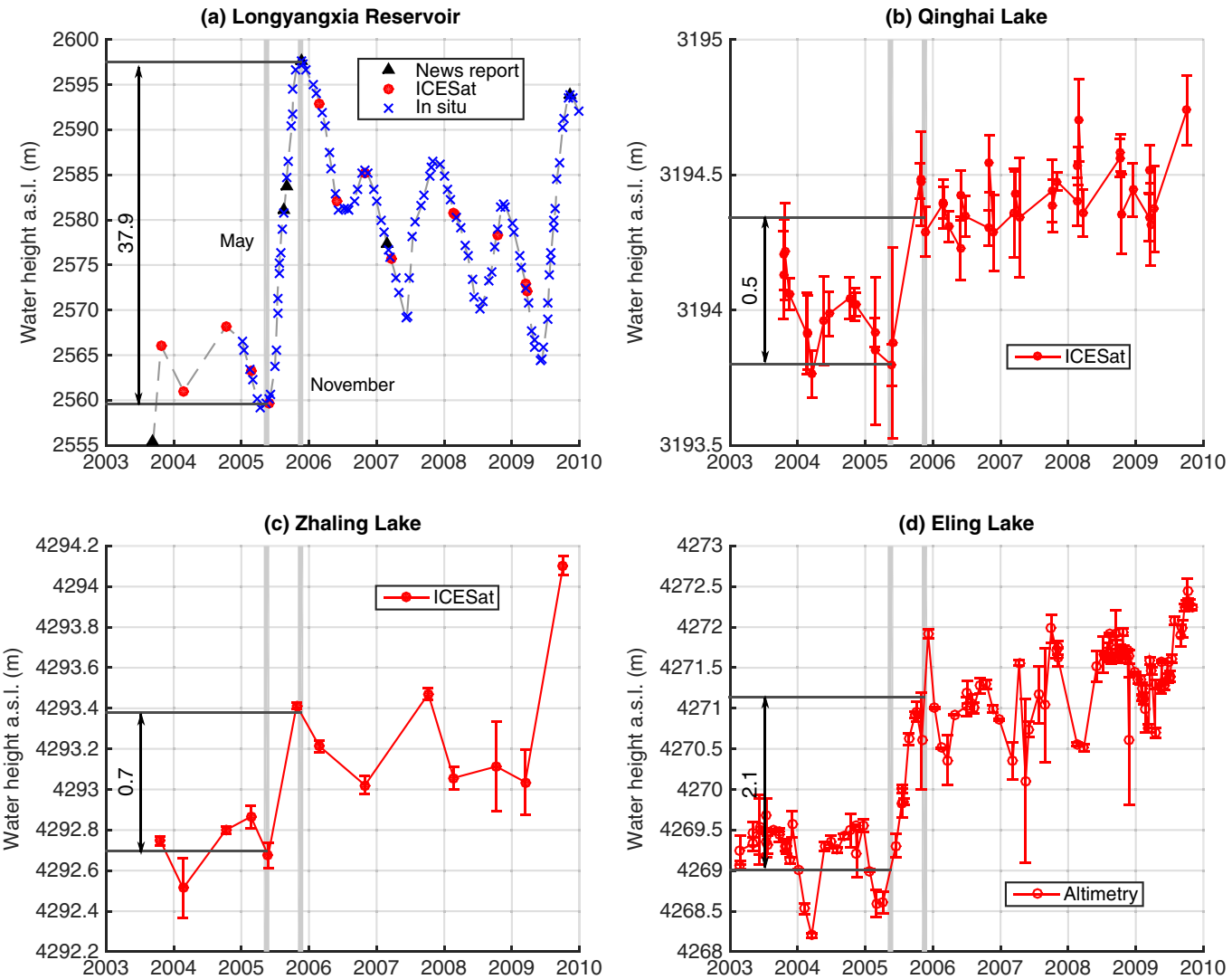

Figure 2. Water level records above sea level (a.s.l.) for the four water bodies. The records are derived from ICESat, altimetry, in situ observations and news reports. The water level rises in the four water bodies between May 2005 and November 2005 are marked, and their values are annotated.

Table 1. Information for Four Large Water Bodies in the Study Area[a]

Name	Longyangxia Reservoir	Qinghai Lake	Zhaling Lake	Eling Lake
Area (km^2)	383	4583	526	610
Altitude (m)	2570	3194	4293	4270
Water level change[b] (m)	37.9	0.5	0.7	2.1
Mass change[b] (Gt)	13.0	2.3	0.4	1.3

[a]The results are based on Longyangxia Hydropower Project (http://www.chincold.org.cn/dams/rootfiles/2010/07/20/1279253974093926-1279253974095162.pdf) and datasets acquired in this study.
[b]From May 2005 to November 2005.

which can reach up to 15 m. The seasonal variations always reached their trough values in May and their peak values in November, which is likely an integrated effect of artificial controls and natural precipitation.

From May to November in 2005, a rapid water level rise can also be identified within Qinghai Lake, Zhaling Lake, and Eling Lake, the magnitudes of which are 0.5, 0.7, and 2.1 m, respectively (Figure 2). Their records from 2003 to 2009 are separated into two stages by this rapid rising period in 2005, during which time the variations are relatively moderate.

3.1.2. Reconstruction of Water Storage Variations Based on the Reservoir "Height-Area Relationship"

As presented in section 2.3, satellite images with measurements for the LR and the surface level obtained above are combined to derive the area-height relationship in the LR. Continuous area changes in the LR, from 165 to 402 km^2, are derived from the obtained 141 images and are shown in Figure 3a, and the linear regression model is shown in Figure 3b. There is a good linear correlation between the area and height, with an R^2 value of 0.9945.

Once we obtain the relationship between the changes in area and water level, we can derive the missing height observations from the area observations. These two results agree well with each other, but they have different data densities, and there are gaps that can be filled by other observations. The details can be found in supporting information.

3.1.3. Robustness of the Reservoir Water Impoundment Reconstruction Based on the "Height-Area Relationship"

As introduced above, there are two methods that can be used to derive the height-area relationship, and these two methods can be mutually verified. The results of the first method have been presented; here, we test whether the second method can obtain similar results. We adopt a 30 m resolution SRTM digital

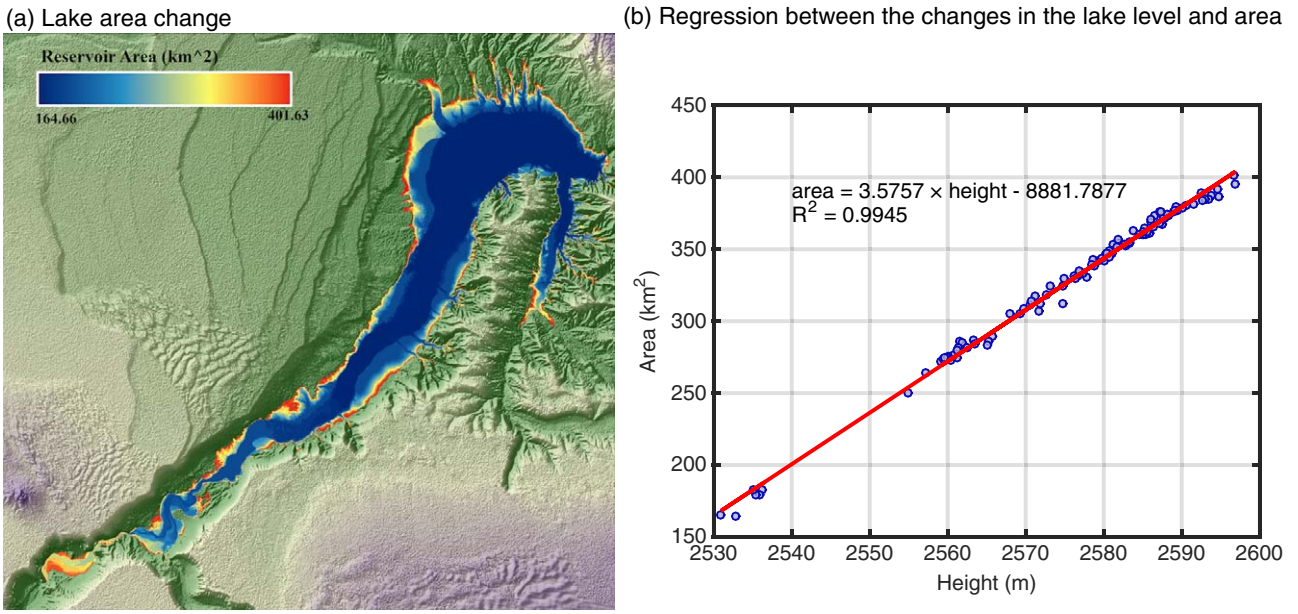

Figure 3. (a) Continuous area changes in the Longyangxia Reservoir derived from remote sensing images. (b) Regression model between the changes in the lake level and area. The linear regression equation is provided in the plot.

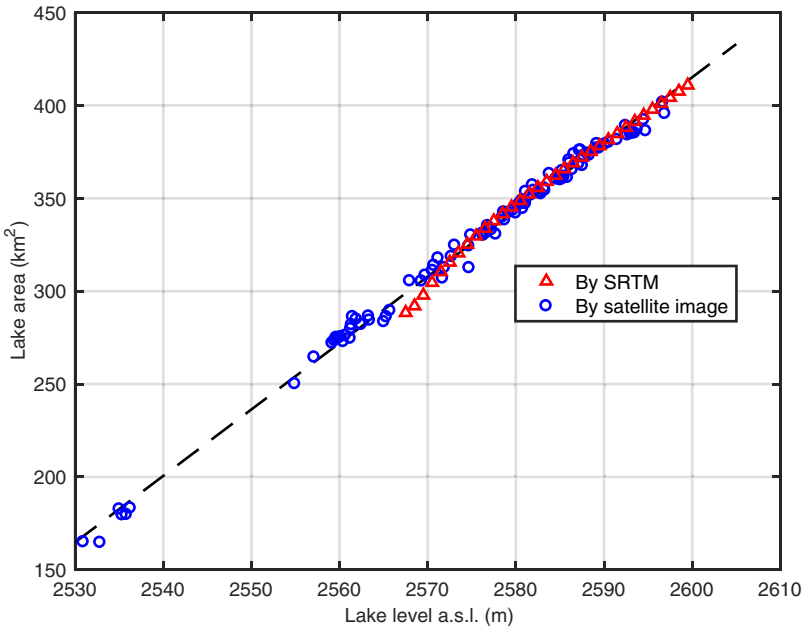

Figure 4. Height-area relationship in the Longyangxia Reservoir obtained using both satellite images and SRTM.

elevation model to simulate how the area of the LR changes with a rise in the water level. The topographic information in our study region was measured in 2000, at which time, the water level of the LR was 2569 m above sea level. The landform under the water is unknown, so we can only simulate the conditions above 2569 m. This method is based on the assumption that lake water will always fill connected spaces at lower elevations if the lake level rises. We simulate the area change for every 1 m rise in the water level, and the results from 2569 to 2600 m are shown in Figure 4. The results obtained using the height-area method have extra observations at low elevations, while the results obtained using topography are more regular. Although the SRTM-derived method tends to generate a smaller area estimation for water levels under 2570 m, these two methods generally agree well with each other, which means that our height-area relationship is reliable.

3.2. Gravimetry of LR Water Impoundment

3.2.1. GRACE-Based Mass Increases Signal Patterns and Comparison With Synthetic Signals

The mask for each water body is shown in the top row in Figure 5. For the case of the LR, its lake area varies with height changes, the corresponding relationship of which is given in Figure 3; therefore, its total mass change is estimated to be 13.0 Gt. The mass increases in the other three lakes are 2.3, 0.4, and 1.3 Gt, respectively (Table 1). Overall, the mass accumulation within these four water bodies is 17.0 Gt, and the LR accounts for 76.5%.

The synthetic EWH changes are shown in the second row of Figure 5. After expansion and truncation, the strength of the EWH of each water body is greatly reduced. Generally, smaller spatial ranges for a signal source indicate that more strength will be attenuated. Here the truncated EWH signal strength in the LR is over 400 times smaller, while that in Qinghai Lake is less than 40 times smaller. Because a smoothing method is often adopted to suppress noise in GRACE observations, we also provide results using a 300 km Gaussian smoothing filter (G300) in the bottom row of Figure 5. The strength of the EWH is further attenuated when using the G300 filter.

GRACE solutions obtained from three different organizations (the CSR, GFZ, and JPL) and using three different filters (DDK4, P4M6+G150, and G300) are used to confirm the EWH changes between May 2005 and November 2005, which is when the water level rapidly increases. There are nine combinations in total, the results for which are shown in Figure 6, together with synthetic signals (the sum of the four sources in Figure 5) produced under the same filters. The smoothing effects increases from the top row to the bottom row in Figure 6, so the synthetic EWH signal decreases. Here we only simulate the water level increase for

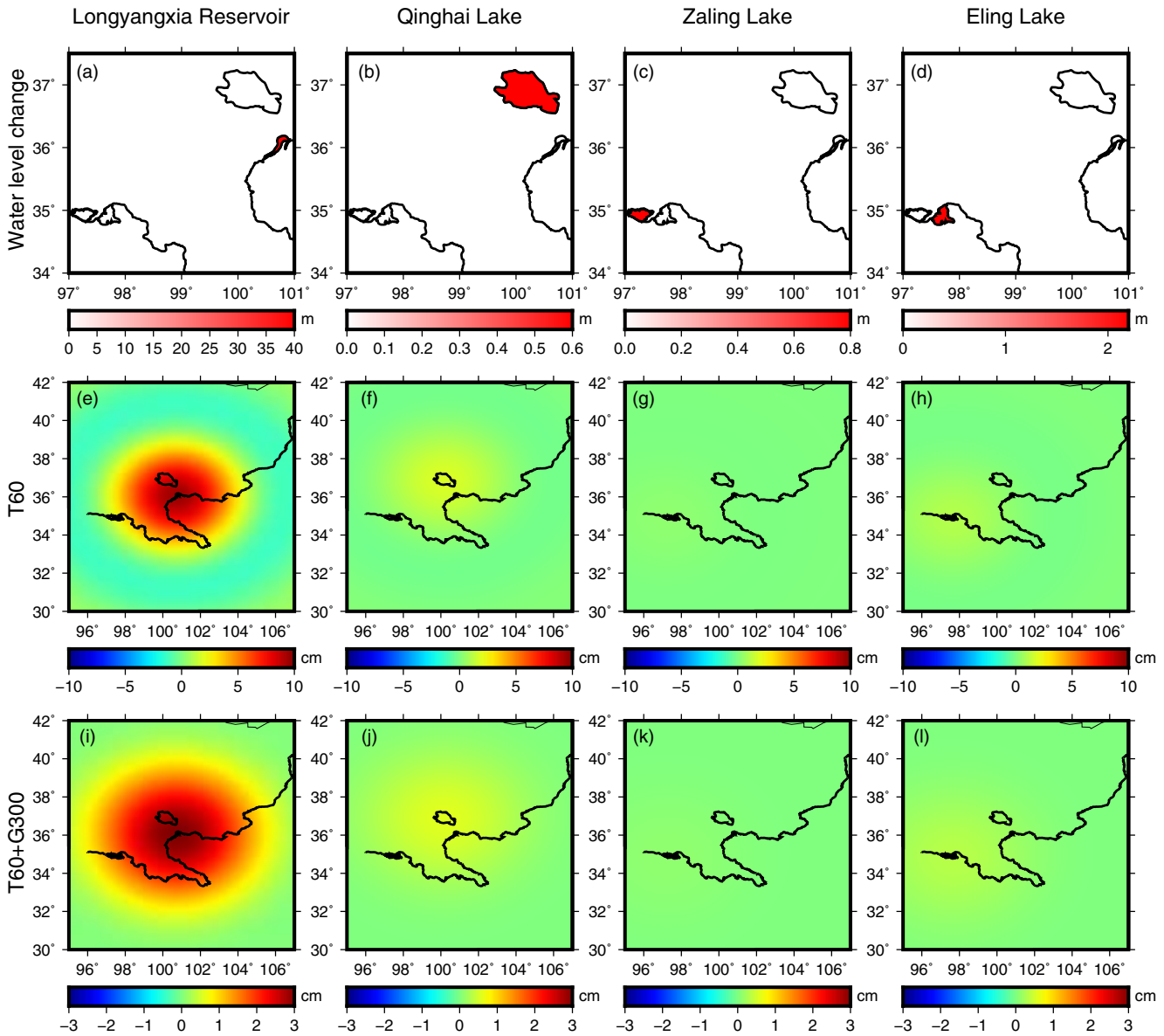

Figure 5. Water level rises for the four water bodies (top) and their calculated gravity effects (middle and bottom). T60: truncated at a degree of 60. T60+G300: truncated at a degree of 60 with a 300 km Gaussian filter. Note that different color scales are used.

the four water bodies. There are other EWH signals caused by the surrounding environment and noise within GRACE solutions, so GRACE observations may be very different from the simulations. There exists a large discrepancy among the different solutions. Among all nine results, the solutions from the CSR with the DDK4 and P4M6+G150 filters demonstrate the best resemblance with the simulations. All solutions using DDK4 contain expected positive EWH signals around the LR, which indicates that DDK4 is more efficient than the other two filters in this case study. Solutions from the GFZ exhibit dominant north-south-oriented striped noise regardless of whether P4M6+G150 or G300 is applied, similar to the JPL solution with the G300 filter. It is noted that G300 is such a strong filter that the synthetic EWH observation is very weak, and thus, the strong positive signal in Figure 6i is clearly a result of noise rather than mass accumulation within the four water bodies. Solutions from the JPL with DDK4 and P4M6+G150 are barely satisfactory. Their shapes are similar enough to the simulations, but their magnitudes are significantly stronger. Based on the discussions above, the CSR solution with the DDK4 filter is chosen for the following research.

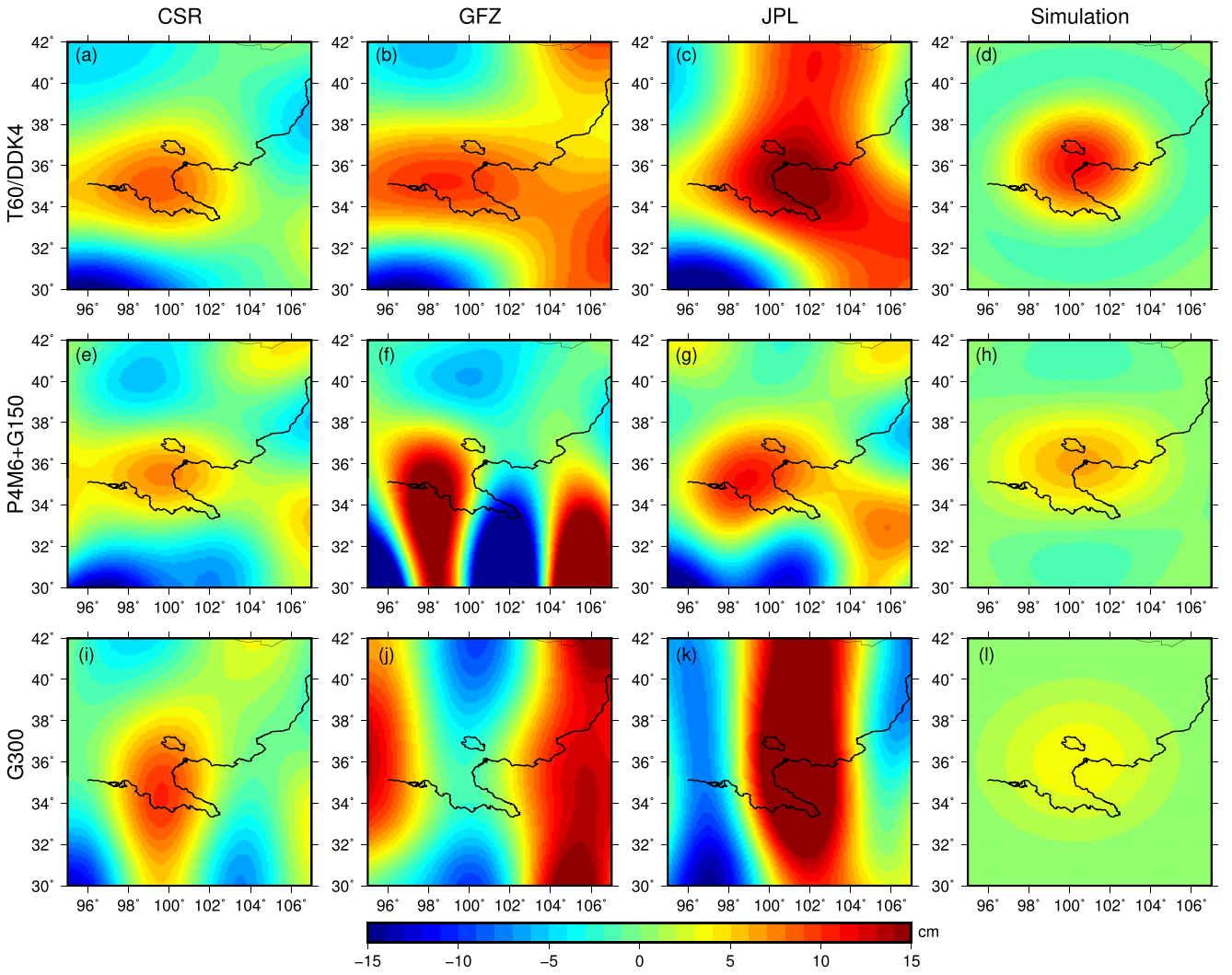

Figure 6. Gravity signals derived from solutions of the GRACE observations (the CSR, GFZ, and JPL) and synthetic gravity changes between the two epochs (May 2005 and November 2005) as marked in Figure 2. Different smoothing methods are compared. T60/DDK4: DDK4 is used for the GRACE solutions, and T60 is used for the simulation. P4M6+G150: a combination of the decorrelation filter P4M6 and a 150 km Gaussian filter. G300: a 300 km Gaussian filter.

3.2.2. The Impoundment Cycle in the LR As Observed by GRACE

Monthly EWH observations from GRACE are presented in Figure 7. The average EWH over the first 4 months in 2005 is taken as the reference and is deducted from all the plots. Based on the water level records in Figure 2, the EWH signals are expected to increase subsequent to May 2005, reach a maximum in November 2005, and decrease afterward. These consecutive observations approximately demonstrate the evolution of the EWH mainly as a consequence of water impoundment in the LR. The positive EWH anomalies are generally discernible following July 2005, except in December 2005. The observations in December 2005 are greatly polluted by north-south-oriented striped noise. It is speculated that a strong negative striped noise runs across the study area (the black dashed curve in Figure 7h) and offsets the expected positive signal. The positive signal grows from January 2006 to March 2006 contradictory to what is expected, and uncertainties either in the GRACE observations or other signal sources (e.g., seepage and soil moisture) are likely to be responsible.

3.2.3. Comparison of Monthly GRACE Signals and Synthesized LR Water Level Time Series

Joint water level changes obtained in this study (supporting information Figure S2) are adopted to simulate EWH changes in the LR (Figure 8a). The position used for calculation is marked with a white star in Figure 7. Gravity effects in the other three lakes are thought to be negligible because of their farther distances and

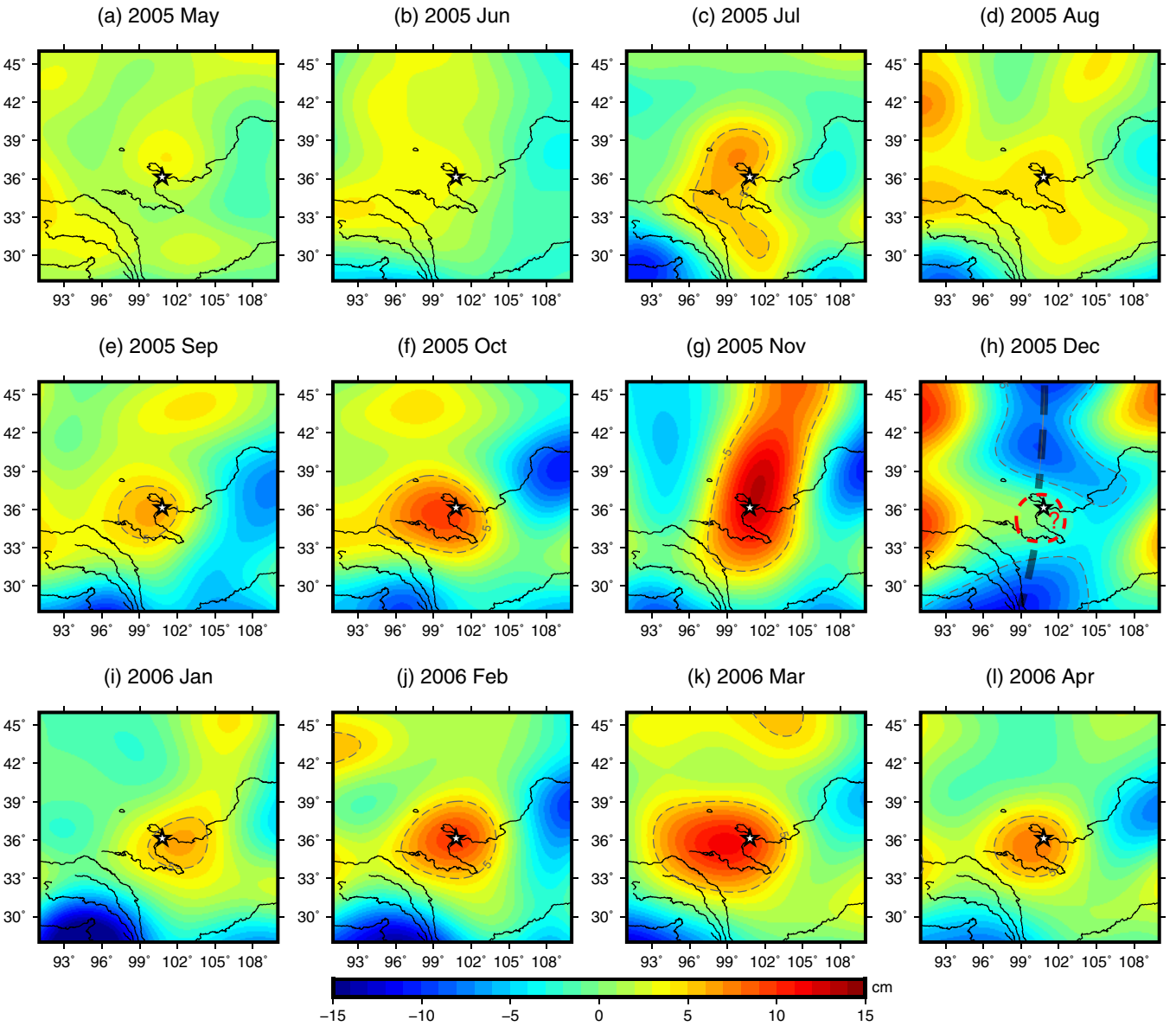

Figure 7. Monthly gravity changes with seasonal variations removed during the period from May 2005 to April 2006 derived from the CSR solutions with a DDK4 filter. All the plots have been deducted from the average of the first 4 months in 2005. The location of the Longyangxia Reservoir is marked with a white star. It is speculated that in December 2005, a strong negative north-south-striped noise overlapped the expected positive signal (marked by the red dashed circle) around the Longyangxia Reservoir.

smaller magnitudes. GRACE observations in the same location are also shown, and data in July 2004, September 2004, and December 2005 are taken as outliers and discarded due to their large discrepancies (green open circles in Figure 8a). Figure 7 shows that the data in 2005 are contaminated by north-south-striped noise. Both of these time series share similar interannual variations and present increasing trends of 1.41 ± 0.15 cm/yr for the GRACE observations and 0.96 ± 0.08 cm/yr for the simulation. The residuals obtained by deducting the GRACE observations from the simulation signals are shown in Figure 8b. We followed the equation given in *Fu and Freymueller* [2012] to quantitatively evaluate the consistency between the GRACE observations and the simulation signal:

$$RMS_{reduction} = \frac{RMS_{GRACE} - RMS_{GRACE-simulation}}{RMS_{GRACE}}.$$

The root mean square (RMS) reduction in this case is 39%, which mainly comes from the consistency within the interannual variation. For reference, *Fu and Freymueller* [2012] implemented a comparison between

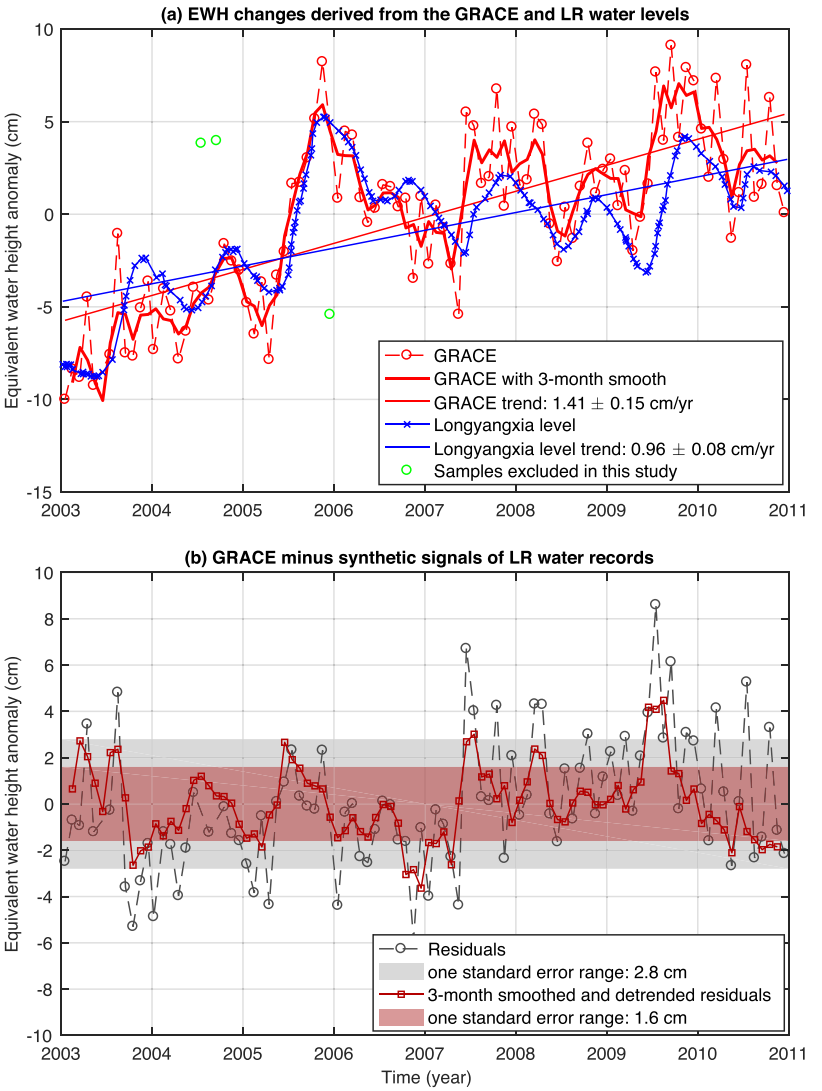

Figure 8. (a) Comparison of the changes in the EWH derived from the CSR solution using DDK4 and in the variations in Longyangxia Reservoir water level and (b) the differences between them. Both the original residuals and the 3 month smoothed and detrended residuals are given. Three outliers (green open circles) are identified and discarded in the analysis. The location used for the calculation is marked with a black star in Figure 7.

GRACE and GPS in Nepal, the results of which were nearly 45%. However, it should be noted that the consistency in their study was mainly concerned with seasonal variation, which is easier to reach because of its strong and regular repeatability. The variations and the remaining trend of 0.5 cm/yr in the residuals may be caused by other signal sources (e.g., soil moisture, seepage, and tectonic process [*Yi et al.*, 2016a]) and/or uncertainties in the GRACE products. We believe these possibilities are difficult to determine with our current understanding due to the scarcity of in situ observations to constrain these phenomena. If we conservatively attribute all the residuals to GRACE uncertainties, the standard deviation of the GRACE observations in this study location is estimated to be 2.8 cm, which is greater than 70% of the residuals. The GRACE series are also smoothed using a three-month sliding window to depress the roughness within the temporal variation, after which their correlation with the synthetic variations is improved from 0.80 to 0.89. The RMS reduction is increased to 53% in this case. If we further assume that the remaining trend originates from the surrounding environment and consequently remove it, the RMS reduction will be increased to 62%, and the GRACE error for the 3-month smoothed value is 1.6 cm (the red curve and red patches in Figure 8b). Note that the GRACE error is a function of both the study area and latitude [*Yi et al.*, 2016c].

Usually, scholars have adopted posterior errors obtained from fitting the residuals of time series, and this method assumes that no systematic error exists within the GRACE solutions. Here we present another way to validate the GRACE errors with the assistance of known signal sources, and its value is better than 2.8 cm at a single point at a latitude of 36°.

4. Discussion

4.1. Detectability of GRACE Data for Arbitrary Signal Sizes

Although GRACE products have a spatial resolution of approximately 100,000 km^2 (truncated at a degree of 60), they can be applied to mass transportation at smaller scales on the condition that their gravity signals are significant enough. To be significant, a signal must be at least stronger than the noise level of the GRACE solutions (the dashed curves in Figure 9a, based on the method presented in *Wahr et al*. [2006]) and must also be stronger than the surrounding signals generated by other sources. For this investigation of the LR, the low precipitation in the study area facilitates detection using GRACE data. The monthly uncertainties of the GRACE solutions are functions of the latitude and have smaller values at higher latitudes. For instance, their EWH values are approximately 3 cm with a 300 km Gaussian filter at a latitude of 30° [*Yi et al*., 2016c], and thus, the maximum EWH of a detectable mass located at a latitude of 30° must be larger than 3 cm. Please note that repeated observations could largely reduce this uncertainty. For example, if 12 months worth of observations within a year are averaged, the uncertainty is expected to be reduced by a factor of $\sqrt{12}$.

The blue and red solid curves in Figure 9 represent the mass required to generate an EWH signal with a maximum value of 1 cm when it is uniformly distributed across an arbitrary area without and with G300, respectively. It is apparent that G300 will attenuate the signal such that a larger mass is needed compared with the observation without G300 for the same size. The noise levels of the CSR products under G300 and DDK4 are presented as dashed curves. In addition to these curves, there are also several known signals representing ice melting and groundwater depletion [*Chen et al*., 2007; *Rodell et al*., 2009; *Famiglietti et al*., 2011; *Feng et al*., 2013; *Gardner et al*., 2013; *Voss et al*., 2013]. Although the maximum EWH values of some signals are far below the noise level, they can still be detected because the uncertainty of GRACE trend can be continuously reduced with the inclusion of additional observations.

The first conclusion is that the required mass for a maximum EWH of 1 cm does not vary much when the size area is smaller than 10,000 km^2 (1° by 1°). To understand this characteristic, a fixed mass of 13 Gt is uniformly attributed to different sizes of areas ranging from 400 to 1,000,000 km^2. The masses are distributed rotational-symmetrically (i.e., a disk) around the North Pole, and thus, when these masses are expanded into SHCs, only the C_{l0} products are nonzero, and their amplitude time series for different orders are shown in Figure 9b (referred to as the range from L0.2 to L10 in the figure). Similar plots and relevant formulas can be found in *Swenson and Wahr* [2002]. Lower degrees represent wider spatial scales, so most of the amplitudes at L10 are located at low degrees. It is interesting that all the series share similarly low degree patterns, while series from wider areas have weaker amplitudes at higher degrees. If the series are truncated at degree 60, it is almost impossible to distinguish between L0.2, L0.7, or L1. The amplitude of each series is proportional to the total mass. Because each of the series are derived from the same amount of mass (13 Gt), they share a similar low degree pattern, which implies that the details about the mass distribution are indistinguishable at such low degrees. Please note that the total mass is only determined by a degree of 0, while the other terms only put an influence on the distribution of the mass. A higher amplitude in one particular degree only means a more elaborate mass distribution rather than a heavier mass.

The second conclusion is that for a smaller range spanned by a signal, a smaller mass is needed to generate a fixed EWH change. Figure 9c shows why the gravitational attraction of a fixed mass to GRACE will decrease when its area is expanded. This decrease is because the increasing horizontal components counteract with each other and the remaining vertical component decreases. This produces an interesting conclusion such that under the condition of a fixed mass, smaller spatial ranges covered by the mass correspond to a higher probability that it can be detected by GRACE data. This conclusion is counterintuitive at first glance because GRACE is mostly used in studies with large signal sizes. This phenomenon is explained in two aspects. First, we should be aware that the area parameter does not exist in the formula of universal gravitation (i.e., only mass and distance are pertinent), so a mass of a smaller size will definitely

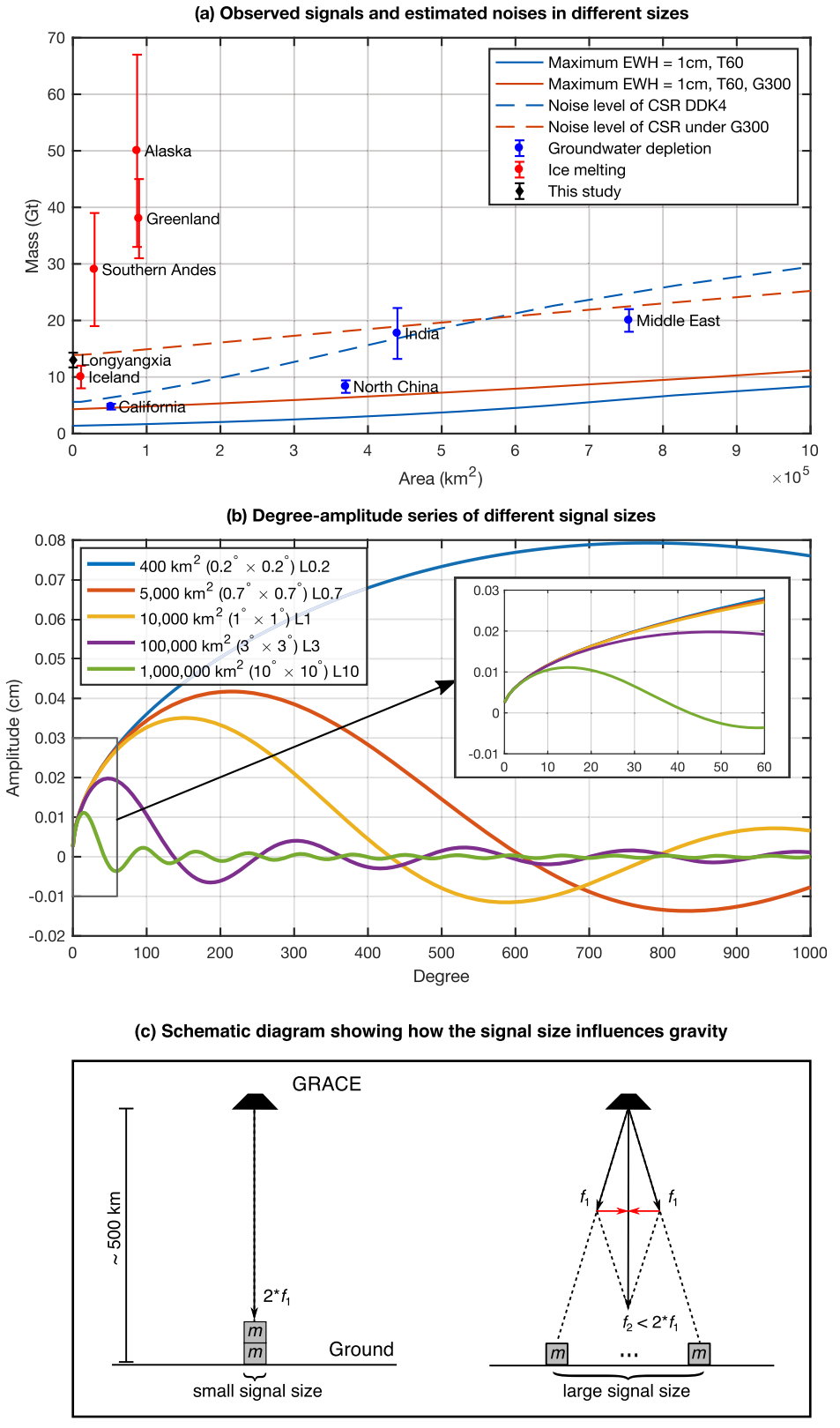

Figure 9. Influence of area and mass on gravity. (a) Observed signals and estimated noise in different sizes. The mass is assumed to be uniformly distributed within an arbitrary size. (b) Degree-amplitude series of different signal sizes with a fixed mass of 13 Gt. The different series are referred to as L0.2, L0.7, L1, L3, and L10. Series in degrees from 0 to 60 are magnified in the inset. The signal spatial sizes are annotated in the legend and their approximate sizes in degrees are converted in the brackets. (c) Schematic diagram that shows why a fixed mass has a weaker attraction to GRACE data when it covers a larger area. The red arrows show that the horizontal components are counteracted with each other.

not have a weaker gravitational force on GRACE satellites. In contrast, its gravity signal may increase, as is shown in Figure 9a and explained in Figure 9c. Second, although the required mass to generate an EWH change above the noise level is reduced for a smaller size object, its EWH will increase sharply with a decrease in its size. In this study, a mass of 13 Gt over an area of 400 km^2 is caused by a water level rise of 37.9 m, which is very uncommon in nature even with the influence of human actions.

The standard to check whether a regional signal can be significantly detected by GRACE data can also be found in Figure 9a. For instance, when the signal area is smaller than 10,000 km^2 (1° by 1°), the noise level of the CSR is approximately 6 Gt under DDK4 and approximately 14 Gt under G300. This value will be even larger if the surrounding gravity signals are more substantial. A low latitude location and a larger spatial size will both increase the difficulty for detection using GRACE data. If the mass change is smaller than these criteria but persists for a long time or continues to grow, it still has a chance to be detectable. Of course, it should be noted that the uncertainties within GRACE data vary from month to month and place to place.

4.2. Analyses of Climate-Induced Dramatic Water Impoundment Within the LR

The reservoir started its initial impoundment in 1986 (Figure 10a). Monthly precipitation records between 1985 and 2010 are shown in Figure 10b. The annual variation and mean precipitation over the entire period are removed, and thus, only the anomalies are shown. Their average values from May to August in each year are compared with the water level changes in Figure 10a. The water level records show a strong interannual variation, which is apparently influenced by precipitation. Four declining periods are identified (with a light red background in Figure 10a) and are directly connected with periods of corresponding insufficient precipitation. One notable phenomenon is that the water level always shows a prompt response to

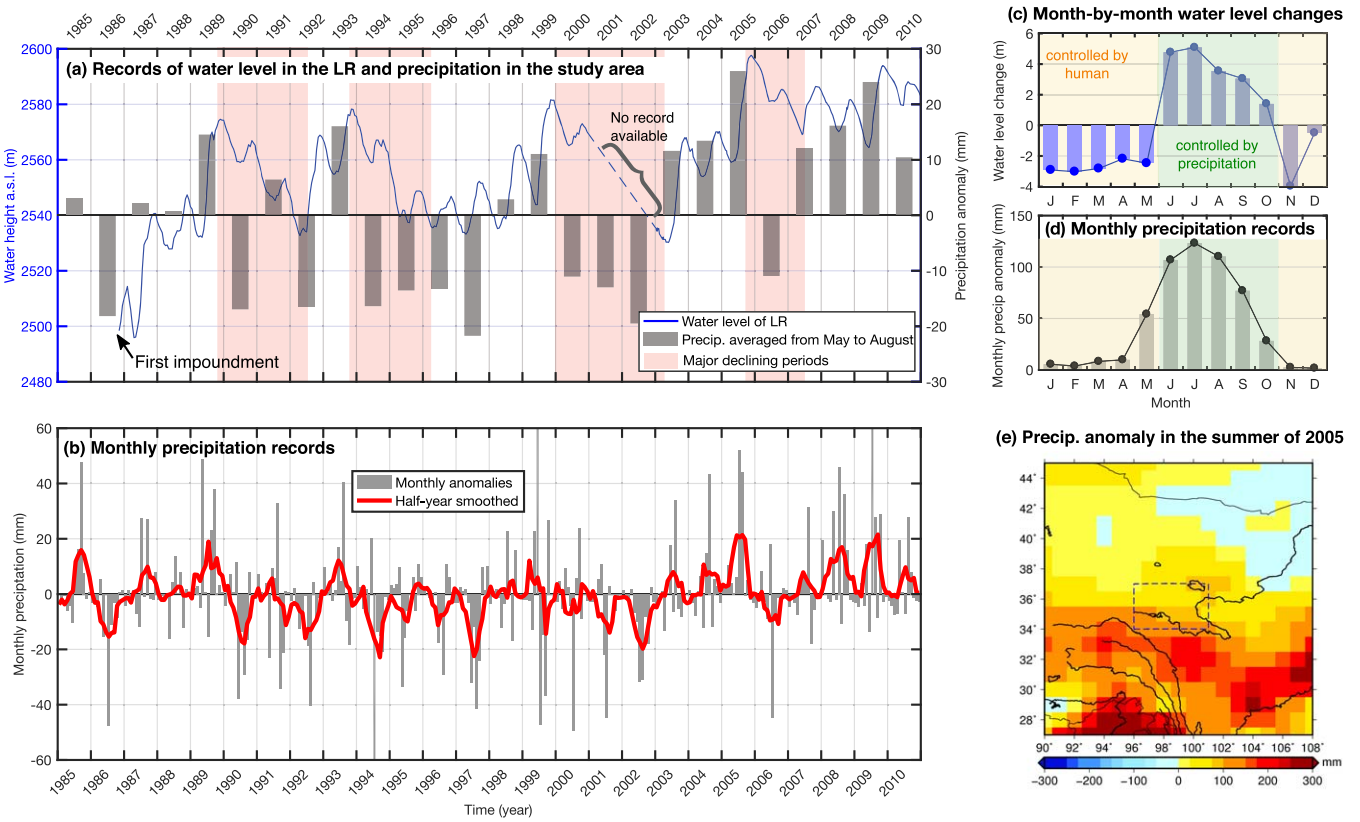

Figure 10. Comparisons of records of the water level in the Longyangxia Reservoir (LR) and precipitation in this region. (a) Records of the water level in the LR from the end of 1986 (when the initial impoundment occurred) to 2010 and of the averaged contemporary precipitation from May to August in each year. There are no water level data available in 2001 or 2002. Four major declining periods are annotated with light red backgrounds. (b) Monthly precipitation records and their half-year smoothed time series. Through a comparison between (c) month-by-month water level changes in the LR and (d) monthly precipitation records, both human-controlled months and precipitation-controlled months are identified. The month-by-month water level change in January is obtained using the difference between the values from February and from January, and so forth. (e) Precipitation anomaly in the summer of 2005 (from July to September) relative to the average precipitation between 2000 and 2010 with the annual variation removed. The dashed box is set as the study region for the precipitation time series.

extensive precipitation, but it exhibits a prolonged response to insufficient precipitation. When we refer to an excess or scarcity in precipitation, it actually concerns only the weather conditions between May and October because precipitation is always scarce during the other months (Figure 10d) and because the LR acts as a supplementary source for the local and downstream water system during these months. This finding means that when encountering a dry summer, the LR must sustain the environment for at least one and a half years. This finding explains the prolonged behavior over these four declining periods and highlights the role of a reservoir in neutralizing floods and droughts, especially within this study region, where precipitation is extremely concentrated during the summer and experiences large interannual variations.

Month-by-month water level changes in the LR are compared with the monthly precipitations in Figures 10c and 10d. There is a good consistency between them from June to October, and thus, we define these months as precipitation controlled. The other months are defined as human controlled. One evidence for this result is that the first 5 months of the year share a similar declining trend, which is likely to be a behavior resulting from artificial planning. We also separate the water level records within each year into rising and declining years (supporting information Figure S3), and we find that the rising years experience abundant precipitation from May to August, while the declining years experience rather scarce precipitation in July.

To summarize, we demonstrate that the water levels in the LR are controlled by both climate and humans. The former determines how the water level rises during wet seasons, and the latter determines how it declines during dry seasons. The highest water level on record in 2005 is explained by the excess precipitation in the summer of 2005. The spatial distribution of the precipitation anomaly in the summer of 2005 is shown in Figure 10e, in which there is a positive anomaly covering the entire eastern Tibetan Plateau. This result implies that the summer of 2005 was a wet season that influenced a much wider range than our study region. The extremely wet months spanning from June to September in 2005 (Figure 10b) caused the rapid water level rise in the LR, which reached its highest level in November. Similar precipitation results were revealed by *Wang et al*. [2016], who showed that the 2005 wet summer caused water storage expansions in many lakes in northeastern Tibet. The surplus summer precipitation in 2009 also caused another simultaneous water storage increase in the four bodies of water, as shown in Figure 2. In conclusion, the simultaneous water storage increase in these four water bodies was mainly the result of surplus precipitation during the summer of 2005.

5. Conclusions

In this work, we investigate the detectability of GRACE data in water storage changes in the ~400 km^2 LR. To examine the mass changes caused by water level rises, we combined observations of Landsat imagery, ICESat, radar altimetry, and in situ measurements to derive the area-height relationship of the LR. We also investigate another independent method based on an SRTM digital elevation model to derive this relationship, and these two methods show good consistency. The rise in the water level to 37.9 m from the summer to the winter of 2005 resulted in a mass increase of 13.0 Gt, the monthly evolution of which is well detected by the CSR solutions with the DDK4 filter. The time series of the EWH changes in the LR, which demonstrate the process of mass accumulation, are also given. After removing the synthetic signals caused by the observed volume changes using GRACE EWH observations from 2003 to 2010, the RMS reduction is 39%. The residuals have a standard deviation of 2.8 cm and a trend of 0.5 cm/yr, which is a combined result of the surrounding soil moisture, seepage effect, tectonic processes, and GRACE errors. The GRACE series show a better resemblance with the synthetic EWH changes in the LR (with a correlation coefficient of 0.89) if the GRACE series are smoothed with a 3 month sliding window.

By a comparison of the interannual and annual terms between water level changes in the LR and precipitation records from 1986 to 2010, we postulate that the water level in the LR is dominated by precipitation during wet seasons and controlled by humans during dry seasons and that the extremely wet summer is responsible for the 2005 highest water level of the LR on record. We also highlight the important role of the LR in the neutralization of floods and droughts.

To date, the LR may be the smallest signal source by surface area reported to be detected by GRACE. This case of the LR decreases the size of research objects of GRACE from previous several times smaller than GRACE solutions to approximately 250 times smaller. A signal with a small size could also be detected by

GRACE given that its mass change is strong enough (6 Gt for the CSR solution with DDK4 or 14 Gt for the CSR solution using G300), and there is little intervention from noise within the surrounding environments. With respect to the LR, we think that such a large water storage change in a semiarid region is a rare case. In the end, we demonstrate that a fixed amount of mass is more likely to be detected by GRACE data when it is more concentrated (i.e., covers a smaller area), but if the size is smaller than 1° by 1°, the ability of the signal to be observed by GRACE will not change even if it is further concentrated.

Acknowledgments
The authors are grateful for publicly accessible GRACE solutions from CSR, GFZ, and JPL, which are available at ICGEM (http://icgem.gfz-potsdam.de/ICGEM/), Landsat images from USGS (http://glovis.usgs.gov), and ICESat data from NASA (http://icesat.gsfc.nasa.gov/icesat/). All data sources are summarized in supporting information Table S1. This research was supported financially by the NSFC (41331066 and 41474059), CAS/CAFEA program (KZZD-EW-TZ-19), Key Research Program of Frontier Sciences CAS (QYZDY-SSW-SYS003), and JSPS KAKENHI grant JP16F16328.

References

Barthelmes, F., and W. Köhler (2016), *The geodesists handbook 2016*, *J. Geod.*, *90*(10), 907–1205, doi:10.1007/s00190-016-0948-z.
Becker, M., W. Llovel, A. Cazenave, A. Güntner, and J.-F. Crétaux (2010), Recent hydrological behavior of the East African great lakes region inferred from GRACE, satellite altimetry and rainfall observations, *C. R. Geosci.*, *342*(3), 223–233, doi:10.1016/j.crte.2009.12.010.
Bettadpur, S. (2012), GRACE level-2 gravity field product user handbook, GRACE 327-734 (CSR-GR-03-01), Center for Space Research, The University of Texas at Austin, Tex.
Birkinshaw, S., G. O'Donnell, P. Moore, C. Kilsby, H. Fowler, and P. Berry (2010), Using satellite altimetry data to augment flow estimation techniques on the Mekong River, *Hydrol. Processes*, *24*(26), 3811–3825.
Boening, C., J. K. Willis, F. W. Landerer, R. S. Nerem, and J. Fasullo (2012), The 2011 La Niña: So strong, the oceans fell, *Geophys. Res. Lett.*, *39*, L19602, doi:10.1029/2012GL053055.
Cao, G. (2004), A character analysis on the deformation of Longyangxia Dam, master thesis, Tianjin Univ., Tianjin, China.
Cazenave, A., K. Dominh, S. Guinehut, E. Berthier, W. Llovel, G. Ramillien, M. Ablain, and G. Larnicol (2009), Sea level budget over 2003–2008: A reevaluation from GRACE space gravimetry, satellite altimetry and Argo, *Global Planet. Change*, *65*(1), 83–88.
Chao, B. F., Y. Wu, and Y. Li (2008), Impact of artificial reservoir water impoundment on global sea level, *Science*, *320*(5873), 212–214.
Chen, J., et al. (2007), Patagonia icefield melting observed by gravity recovery and climate experiment (GRACE), *Geophys. Res. Lett.*, *34*, L22501, doi:10.1029/2007GL031871.
Chen, J., C. Wilson, and B. Tapley (2013), Contribution of ice sheet and mountain glacier melt to recent sea level rise, *Nat. Geosci.*, *6*(7), 549–552.
Chen, J. L., C. R. Wilson, D. Blankenship, and B. D. Tapley (2009), Accelerated Antarctic ice loss from satellite gravity measurements, *Nat. Geosci.*, *2*(12), 859–862, doi:10.1038/ngeo694.
Chen, J. L., C. R. Wilson, B. D. Tapley, B. Scanlon, and A. Güntner (2016), Long-term groundwater storage change in Victoria, Australia from satellite gravity and in situ observations, *Global Planet. Change*, *139*, 56–65, doi:10.1016/j.gloplacha.2016.01.002.
Cheng, M., J. C. Ries, and B. D. Tapley (2011), Variations of the Earth's figure axis from satellite laser ranging and GRACE, *J. Geophys. Res.*, *116*, B01409, doi:10.1029/2010JB000850.
Church, J. A., P. U. Clark, A. Cazenave, J. M. Gregory, S. Jevrejeva, A. Levermann, M. A. Merrifield, G. A. Milne, R. S. Nerem, and P. D. Nunn (2013), Sea level change, in *Climate Change 2013: The Physical Science Basis*, edited by T. F. Stocker, et al., Cambridge Univ. Press, Cambridge, U. K.
Crétaux, J.-F., W. Jelinski, S. Calmant, A. Kouraev, V. Vuglinski, M. Bergé-Nguyen, M.-C. Gennero, F. Nino, R. A. Del Rio, and A. Cazenave (2011), SOLS: A lake database to monitor in the near real time water level and storage variations from remote sensing data, *Adv. Space Res.*, *47*(9), 1497–1507.
Duan, Z., and W. Bastiaanssen (2013), Estimating water volume variations in lakes and reservoirs from four operational satellite altimetry databases and satellite imagery data, *Remote Sens. Environ.*, *134*, 403–416.
Famiglietti, J., M. Lo, S. Ho, J. Bethune, K. Anderson, T. Syed, S. Swenson, C. de Linage, and M. Rodell (2011), Satellites measure recent rates of groundwater depletion in California's Central Valley, *Geophys. Res. Lett.*, *38*, L03403, doi:10.1029/2010GL046442.
Farinotti, D., L. Longuevergne, G. Moholdt, D. Duethmann, T. Mölg, T. Bolch, S. Vorogushyn, and A. Güntner (2015), Substantial glacier mass loss in the Tien Shan over the past 50 years, *Nat. Geosci.*, *8*, 716–722.
Farr, T. G., P. A. Rosen, E. Caro, R. Crippen, R. Duren, S. Hensley, M. Kobrick, M. Paller, E. Rodriguez, and L. Roth (2007), The shuttle radar topography mission, *Rev. Geophys.*, *45*, RG2004, doi:10.1029/2005RG000183.
Feng, W., M. Zhong, J. M. Lemoine, R. Biancale, H. T. Hsu, and J. Xia (2013), Evaluation of groundwater depletion in North China using the Gravity Recovery and Climate Experiment (GRACE) data and ground-based measurements, *Water Resour. Res.*, *49*, 2110–2118, doi:10.1002/wrcr.20192.
Frappart, F., F. Papa, A. Güntner, W. Susanna, G. Ramillien, C. Prigent, W. B. Rossow, and M.-P. Bonnet (2010), Interannual variations of the terrestrial water storage in the Lower Ob'Basin from a multisatellite approach, *Hydrol. Earth Syst. Sci. Discuss.*, *14*(12), 2443–2453.
Frappart, F., F. Papa, A. Güntner, S. Werth, J. S. Da Silva, J. Tomasella, F. Seyler, C. Prigent, W. B. Rossow, and S. Calmant (2011), Satellite-based estimates of groundwater storage variations in large drainage basins with extensive floodplains, *Remote Sens. Environ.*, *115*(6), 1588–1594.
Fu, Y., and J. T. Freymueller (2012), Seasonal and long-term vertical deformation in the Nepal Himalaya constrained by GPS and GRACE measurements, *J. Geophys. Res.*, *117*, B03407, doi:10.1029/2011JB008925.
Gardner, A. S., et al. (2013), A reconciled estimate of glacier contributions to sea level rise: 2003 to 2009, *Science*, *340*(6134), 852–857, doi:10.1126/science.1234532.
Huang, Y., S. Salama, M. S. Krol, Z. Su, A. Y. Hoekstra, Y. Zeng, and Y. Zhou (2015), Estimation of human-induced changes in terrestrial water storage through integration of GRACE satellite detection and hydrological modeling: A case study of the Yangtze River basin, *Water Resour. Res.*, *51*, 8494–8516, doi:10.1002/2015WR016923.
Kusche, J., R. Schmidt, S. Petrovic, and R. Rietbroek (2009), Decorrelated GRACE time-variable gravity solutions by GFZ, and their validation using a hydrological model, *J. Geod.*, *83*(10), 903–913.
Landerer, F., and S. Swenson (2012), Accuracy of scaled GRACE terrestrial water storage estimates, *Water Resour. Res.*, *48*, W04531, doi:10.1029/2011WR011453.
Leon, J. G., S. Calmant, F. Seyler, M.-P. Bonnet, M. Cauhopé, F. Frappart, N. Filizola, and P. Fraizy (2006), Rating curves and estimation of average water depth at the upper Negro River based on satellite altimeter data and modeled discharges, *J. Hydrol.*, *328*(3), 481–496.
Li, J., and Y. Sheng (2012), An automated scheme for glacial lake dynamics mapping using Landsat imagery and digital elevation models: A case study in the Himalayas, *Int. J. Remote Sens.*, *33*(16), 5194–5213.
Long, D., Y. Yang, Y. Wada, Y. Hong, W. Liang, Y. Chen, B. Yong, A. Hou, J. Wei, and L. Chen (2015), Deriving scaling factors using a global hydrological model to restore GRACE total water storage changes for China's Yangtze River Basin, *Remote Sens. Environ.*, *168*, 177–193.
Lu, Y. (2013), Analysis of transfusion in G4 cleavage belt of the Longyangxia Reservoir with its water level higher than 2594 m, *QingHai Hydroelectr. Gener.*, *4*, 51–54.

Matgen, P., G. Schumann, J.-B. Henry, L. Hoffmann, and L. Pfister (2007), Integration of SAR-derived river inundation areas, high-precision topographic data and a river flow model toward near real-time flood management, *Int. J. Appl. Earth Obs. Geoinf.*, *9*(3), 247–263.
Matsuo, K., and K. Heki (2010), Time-variable ice loss in Asian high mountains from satellite gravimetry, *Earth Planet. Sci. Lett.*, *290*(1–2), 30–36, doi:10.1016/j.epsl.2009.11.053.
McFeeters, S. K. (1996), The use of the Normalized Difference Water Index (NDWI) in the delineation of open water features, *Int. J. Remote Sens.*, *17*(7), 1425–1432.
Medina, C., J. Gomez-Enri, J. J. Alonso, and P. Villares (2010), Water volume variations in Lake Izabal (Guatemala) from in situ measurements and ENVISAT Radar Altimeter (RA-2) and Advanced Synthetic Aperture Radar (ASAR) data products, *J. Hydrol.*, *382*(1), 34–48.
Pan, F., J. Liao, X. Li, and H. Guo (2013), Application of the inundation area—Lake level rating curves constructed from the SRTM DEM to retrieving lake levels from satellite measured inundation areas, *Comput. Geosci.*, *52*, 168–176.
Peng, D., S. Guo, P. Liu, and T. Liu (2006), Reservoir storage curve estimation based on remote sensing data, *J. Hydrol. Eng.*, *11*(2), 165–172.
Reager, J., A. Gardner, J. Famiglietti, D. Wiese, A. Eicker, and M.-H. Lo (2016), A decade of sea level rise slowed by climate-driven hydrology, *Science*, *351*(6274), 699–703.
Rodell, M., I. Velicogna, and J. S. Famiglietti (2009), Satellite-based estimates of groundwater depletion in India, *Nature*, *460*(7258), 999–1002.
Schneider, U., A. Becker, P. Finger, A. Meyer-Christoffer, B. Rudolf, and M. Ziese (2011), GPCC Full Data Reanalysis Version 6.0 at 1.0°: Monthly Land-Surface Precipitation from Rain-Gauges built on GTS-based and Historic Data, doi:10.5676/DWD_GPCC/FD_M_V7_100. [Available at https://www.esrl.noaa.gov/psd/data/gridded/data.gpcc.html.]
Schutz, B., H. Zwally, C. Shuman, D. Hancock, and J. DiMarzio (2005), Overview of the ICESat mission, *Geophys. Res. Lett.*, *32*, L21S01, doi:10.1029/2005GL024009.
Sheng, Y., C. Song, J. Wang, E. A. Lyons, B. R. Knox, J. S. Cox, and F. Gao (2016), Representative lake water extent mapping at continental scales using multi-temporal Landsat-8 imagery, *Remote Sens. Environ.*, *185*, 129–141.
Singh, A., F. Seitz, and C. Schwatke (2012), Inter-annual water storage changes in the Aral Sea from multi-mission satellite altimetry, optical remote sensing, and GRACE satellite gravimetry, *Remote Sens. Environ.*, *123*, 187–195.
Song, C., and Y. Sheng (2016), Contrasting evolution patterns between glacier-fed and non-glacier-fed lakes in the Tanggula Mountains and climate cause analysis, *Clim. Change*, *135*(3–4), 493–507.
Song, C., B. Huang, and L. Ke (2013), Modeling and analysis of lake water storage changes on the Tibetan Plateau using multi-mission satellite data, *Remote Sens. Environ.*, *135*, 25–35.
Song, C., L. Ke, B. Huang, and K. S. Richards (2015), Can mountain glacier melting explains the GRACE-observed mass loss in the southeast Tibetan Plateau: From a climate perspective?, *Global Planet. Change*, *124*, 1–9.
Swenson, S., and J. Wahr (2002), Methods for inferring regional surface-mass anomalies from Gravity Recovery and Climate Experiment (GRACE) measurements of time-variable gravity, *J. Geophys. Res.*, *107*(B9), 2193, doi:10.1029/2001JB000576.
Swenson, S., and J. Wahr (2006), Post-processing removal of correlated errors in GRACE data, *Geophys. Res. Lett.*, *33*, L08402, doi:10.1029/2005gl025285.
Swenson, S., and J. Wahr (2009), Monitoring the water balance of Lake Victoria, East Africa, from space, *J. Hydrol.*, *370*(1–4), 163–176, doi:10.1016/j.jhydrol.2009.03.008.
Swenson, S., D. Chambers, and J. Wahr (2008), Estimating geocenter variations from a combination of GRACE and ocean model output, *J. Geophys. Res.*, *113*, B08410, doi:10.1029/2007JB005338.
Tseng, K.-H., C. Shum, J.-W. Kim, X. Wang, K. Zhu, and X. Cheng (2016), Integrating Landsat imageries and digital elevation models to infer water level change in Hoover Dam, *IEEE J. Sel. Top. Appl. Earth Obs. Remote Sens.*, *9*(4), 1696–1709.
Velicogna, I., and J. Wahr (2006), Acceleration of Greenland ice mass loss in spring 2004, *Nature*, *443*(7109), 329–331.
Voss, K. A., J. S. Famiglietti, M. Lo, C. Linage, M. Rodell, and S. C. Swenson (2013), Groundwater depletion in the Middle East from GRACE with implications for transboundary water management in the Tigris-Euphrates-Western Iran region, *Water Resour. Res.*, *49*(2), 904–914.
Wahr, J., M. Molenaar, and F. Bryan (1998), Time variability of the Earth's gravity field: Hydrological and oceanic effects and their possible detection using GRACE, *J. Geophys. Res.*, *103*(B12), 30,205–30,229, doi:10.1029/98jb02844.
Wahr, J., S. Swenson, and I. Velicogna (2006), Accuracy of GRACE mass estimates, *Geophys. Res. Lett.*, *33*, L06401, doi:10.1029/2005GL025305.
Wang, H., Z. Wang, and X. Yuan (2007), Water storage changes in Three Gorges water systems area inferred from GRACE time-variable gravity data [in Chinese], *Chin. J. Geophys.*, *50*(3), 730–736.
Wang, J., Y. Sheng, and T. S. D. Tong (2014), Monitoring decadal lake dynamics across the Yangtze Basin downstream of Three Gorges Dam, *Remote Sens. Environ.*, *152*, 251–269.
Wang, Q., S. Yi, and W. Sun (2016), The changing pattern of lake and its contribution to increased mass in the Tibetan Plateau derived from GRACE and ICESat data, *Geophys. J. Int.*, *207*(1), 528–541.
Wang, X., C. de Linage, J. Famiglietti, and C. S. Zender (2011), Gravity Recovery and Climate Experiment (GRACE) detection of water storage changes in the Three Gorges Reservoir of China and comparison with in situ measurements, *Water Resour. Res.*, *47*, W12502, doi:10.1029/2011WR010534.
Wang, X., P. Gong, Y. Zhao, Y. Xu, X. Cheng, Z. Niu, Z. Luo, H. Huang, F. Sun, and X. Li (2013), Water-level changes in China's large lakes determined from ICESat/GLAS data, *Remote Sens. Environ.*, *132*, 131–144.
Xiang, L., H. Wang, H. Steffen, P. Wu, L. Jia, L. Jiang, and Q. Shen (2016), Groundwater storage changes in the Tibetan Plateau and adjacent areas revealed from GRACE satellite gravity data, *Earth Planet. Sci. Lett.*, *449*, 228–239.
Yi, S., and W. Sun (2014), Evaluation of glacier changes in high-mountain Asia based on 10 year GRACE RL05 models, *J. Geophys. Res. Solid Earth*, *119*, 2504–2517, doi:10.1002/2013JB010860.
Yi, S., W. Sun, K. Heki, and A. Qian (2015), An increase in the rate of global mean sea level rise since 2010, *Geophys. Res. Lett.*, *42*, 3998–4006, doi:10.1002/2015gl063902.
Yi, S., J. T. Freymueller, and W. Sun (2016a), How fast is the middle-lower crust flowing in eastern Tibet? A constraint from geodetic observations, *J. Geophys. Res. Solid Earth*, *121*, 6903–6915, doi:10.1002/2016JB013151.
Yi, S., Q. Wang, L. Chang, and W. Sun (2016b), Changes in mountain glaciers, lake levels, and snow coverage in the Tianshan monitored by GRACE, ICESat, Altimetry, and MODIS, *Remote Sens.*, *8*(10), 798, doi:10.3390/rs8100798.
Yi, S., Q. Wang, and W. Sun (2016c), Basin mass dynamic changes in China from GRACE based on a multibasin inversion method, *J. Geophys. Res. Solid Earth*, *121*, 3782–3803, doi:10.1002/2015JB012608.
Zhang, G., H. Xie, S. Kang, D. Yi, and S. F. Ackley (2011), Monitoring lake level changes on the Tibetan Plateau using ICESat altimetry data (2003–2009), *Remote Sens. Environ.*, *115*(7), 1733–1742.
Zhang, G., H. Xie, T. Yao, and S. Kang (2013), Water balance estimates of ten greatest lakes in China using ICESat and Landsat data, *Chin. Sci. Bull.*, *58*(31), 3815–3829.